fire

MDPI

Article

A Study on the Maximum Temperature of a Ceiling Jet of Asymmetric Dual Strong Plumes in a Naturally Ventilated Tunnel

Shenghao Zhang and Na Meng *

College of Safety and Environmental Engineering, Shandong University of Science and Technology, Qingdao 266590, China; 202182200024@sdust.edu.cn
* Correspondence: mengna@sdust.edu.cn

Abstract: This paper explores the temperature distribution (TD) and maximum temperature (MT) below the ceiling induced by the ceiling jet of an asymmetric dual fire sources in a naturally ventilated tunnel. Considering strong plumes, this study investigates the effects of fire size and spacing of asymmetric dual fire sources on TD and MT. With the same power of fire source, when the size of one of the fire sources increases, the corresponding maximum temperature beneath ceiling decreases. Additionally, the temperature peak below the ceiling shifts from one to two, and the peak temperature of the larger fire source is lower compared to that of smaller one. When the fire sources distance increases, the maximum temperature initially decreases and then increases. Beyond a certain distance, the maximum temperature no longer changes with increasing distance. In this study, we investigated the effect of fire source size and spacing on the MT of the tunnel ceiling for asymmetric dual fire sources. A new model for predicting the MT underneath the tunnel ceiling was developed, taking into account the factors as fire spacing and fire size. The model is able to make effective predictions of the simulation results.

Keywords: tunnel fire; asymmetric dual fires; strong plume; fire size; fire spacing; maximum temperature

Citation: Zhang, S.; Meng, N. A Study on the Maximum Temperature of a Ceiling Jet of Asymmetric Dual Strong Plumes in a Naturally Ventilated Tunnel. *Fire* **2024**, *7*, 110. https://doi.org/10.3390/fire7040110

Academic Editors: Kaihua Lu, Jianping Zhang, Jie Wang, Xiaochun Zhang and Wei Tang

Received: 18 February 2024
Revised: 21 March 2024
Accepted: 24 March 2024
Published: 26 March 2024

1. Introduction

The increase in the number and length of tunnels has enhanced transportation efficiency and brought great convenience to urban traffic. However, as the construction and use of tunnels have gradually increased, the risk of tunnel fire accidents, as well as the harm caused by tunnel fires, is increasing [1–7]. Researches indicate that in the event of a tunnel fire, due to its narrow and sealed structural characteristics, the high-temperature flames and toxic smoke generated by the fire can cause significant harm, with temperatures reaching up to 1000 °C and sustaining for extended periods [8,9]. The high-temperature smoke gathered under the tunnel ceiling will not only endanger people's lives and health, but will also damage the tunnel's wall and supporting structure, which can lead to collapses, affecting evacuations and fire rescues [10]. Temperature detection is a key factor in the management of accidental combustion incidents and in the formulation of fire safety designs [11]. Therefore, studying the TD and the MT below the tunnel ceiling is of great significance.

Regarding the MT and TD beneath the tunnel ceiling in the event of a fire, prior research has extensively explored these phenomena through both experimental and numerical simulation methodologies.

Alpert [12] conducted experimental research on the MT of ceiling jet under an open ceiling and developed a predictive model for the MT based on ceiling height and fire source power. Heskestad and Hamada [13] conducted experiments to investigate the TD below the ceiling under strong plume conditions. Based on their findings, they suggested

a model that uses the plume radius as the feature length. Ingason et al. [14] researched the TD and MT of tunnel fires at different ventilation rates by means of reduced-size tunnel experiments. Kurioka et al. [15] carried out experimental research using a variety of tunnel models that varied in size and shape. By varying the longitudinal ventilation speed, the heat release rate, and the aspect ratio of the tunnel cross-section, they conducted studies on the flame height, the MT below ceiling, and its location, and they established a predictive model for the MT below ceiling under longitudinal ventilation conditions. Zhang et al. [16] employed numerical simulations to investigate the MT and the length of smoke back-layering in the downstream direction from the fire source in a tilted tunnel under conditions of natural ventilation. Based on their findings, they developed predictive models for the MT increase and smoke back-layering length in inclined tunnels. Caliendo et al. [17] employed a Computational Fluid Dynamics (CFD) model to simulate fire scenarios within tunnels under natural ventilation conditions, examining the effects of longitudinal slope and traffic volume on fire incidents. Through numerical simulations and a quantitative risk analysis approach, the research pinpointed crucial factors influencing safety outcomes. Ji et al. [18] constructed an equal-size tunnel model for numerical simulation studies. By adjusting the fire source's aspect ratio and heat release rate, they established a model for the longitudinal distribution of smoke temperature beneath the tunnel ceiling. Gao et al. [19] investigated the combustion of a single fire source in tunnels with natural ventilation using numerical simulation methods. They investigated the characteristics of fire combustion in inclined tunnels by varying the tunnel's slope and proposed a correlation for predicting the highest temperature beneath the tunnel ceiling based on their research findings.

The aforementioned studies focus exclusively on single-ignition source combustion in tunnels, whereas in practice, multiple-ignition source combustion is significantly more prevalent. This is particularly evident in scenarios such as traffic accidents within tunnels, when the combustion and subsequent explosion of a vehicle can ignite a fire which can spread to nearby vehicles, causing multiple fire sources. Compared to combustion from one fire source, the burning of multiple fire sources significantly increases the volume of smoke and toxic gases. The combustion of multiple fire sources accelerates the spread of fire, leading to larger-scale incidents. Furthermore, it can cause a rise in temperature and an expansion of the heat radiation zone. According to the above research, it can be concluded that, compared to single fire source, the combustion of multiple fire sources in tunnels presents a greater hazard by increasing the concentration of smoke, accelerating the spread of flame, and elevating temperatures and heat radiation zones. Therefore, preventive and management measures for multiple fire source combustion should be given special attention.

With regard to multiple ignition source combustion in tunnels, the following aspects have been studied by previous researchers.

Zhou et al. [20] conducted an experiment using a scaled tunnel model to investigate the effects of the fire sources distance and the lateral positioning of fire sources on the temperature distribution beneath the tunnel ceiling under natural ventilation conditions. Their study revealed that the longitudinal temperature distribution below ceiling is largely insensitive to the lateral positions of the two fire sources when they are at a given distance apart. They suggested a MT prediction model that considered the separation between the fire sources, as well as their lateral positions. Zhang et al. [21] studied dual fires in a model tunnel. By varying the heat release rate (HRR) of fire sources, the distance between dual fire sources, and the longitudinal ventilation speed within the tunnel, they conducted a detailed study. Based on their testing data, they analyzed the temperature distribution below the tunnel ceiling. Wan et al. [22] studied the MT and TD of the ceiling caused by the combustion of two unequal propane fire sources in a natural ventilation tunnel. Based on the research results, they proposed a new normalized HRR and established a unified model to predict the MT rise below the ceiling for two fire sources. Meng [23] conducted a numerical simulation to investigate the temperature distribution of smoke generated by two fire sources under a natural ventilation scene beneath the tunnel ceiling. The study

investigated the impact of the lateral distance of fire sources on the TD below tunnel ceiling, and constructed a model to predict the TD below ceiling based on the research results. Wang et al.'s study [24] utilized a small-scale tunnel model to analyze the TD at the ceiling of a tunnel burning a pair of identical fire sources under natural ventilation. Through the study, it was discovered that the longitudinal TD below ceiling adheres to an exponential decay law, the temperature decay index K decreases with increasing fire spacing, and a maximum temperature prediction model taking fire power and fire spacing into account was developed. Jia et al. [25] studied dual fires in tunnels by using reduced size tunnel model experiments and numerical simulations. They investigated the TD below ceiling under various conditions by modifying the size (D) and spacing (S) of the two fire sources. According to the insights from the study, an analysis model for the temperature distribution was proposed for cases when the ratio of S/D exceeds 2. Zhao et al. [26] constructed a small-scale tunnel model to investigate the combustion process involving two fire sources within a tunnel, focusing on the longitudinal TD below ceiling by altering the size and spacing of two identical fire sources. Based on these experimental results, they developed models to elucidate both the MT beneath the ceiling and the attenuation of longitudinal temperature. Heidarinejad et al. [27] examined the interactions between dual fire sources and tunnel obstructions, as well as their impact on the critical ventilation velocity, by configuring vehicle models of varying sizes and altering the distances between the vehicles and fire sources.

The research available primarily focuses on tunnel fires involving either one or dual fire sources that are identical in both size and power, with less attention given to asymmetric dual fire sources. However, real tunnel fires often involve multiple fire sources of varying sizes, highlighting the necessity of studying asymmetric dual fire sources. In this paper, we use Fire Dynamics Simulator (FDS 6.7.1) software to create a full size model tunnel. This model investigates the influence of two asymmetric fire sources, which have identical power but vary in size and shape, on the longitudinal TD and the MT below ceiling. The findings from this study are intended to provide insightful information that can assist in emergency response planning and the design of fire prevention measures for tunnels. The relevant research results also have a certain guiding value for fire rescue, providing a reference for similar research.

2. Numerical Simulation

The Fire Dynamics Simulator (FDS), which is based on Computational Fluid Dynamics (CFD) technology, is used in the numerical simulation investigations. FDS 6.7.1 can numerically provide predictions and analyses of fire spread and development. The software additionally includes Smoke-view 6.7.5, a tool that depicts the spread of fire smoke in tunnel fires using various parameters such as visibility and temperature fields. Compared to full-scale and scaled-down experiments, numerical simulation research can provide safer, more economical, controllable, and repeatable analysis and prediction capability. FDS has been used extensively in the study of fires, and a significant body of experimental data has confirmed its dependability [28–34].

2.1. Numerical Modelling of Tunnels

A numerical model (with size of 200 m $\times$ 10 m $\times$ 5 m) was created. Two rectangular fire sources, denoted as burner A and B, were used, with heptane as fuel. Based on the fire source size used in previous tunnel fire research [35], burner A's width and height were set as 1 m, with length setting as 1 m, 1.2 m, 1.5 m, 1.8 m, and 2 m. Burner B's dimensions were fixed at 1 m in all three dimensions. The fire sources were located along the tunnel's longitudinal midline, while the distance between the edges of the two fire sources were adjusted to change the fire spacing from 0 m to 2 m. To detect the longitudinal temperature distribution beneath ceiling, a number of thermocouples were inserted. The longitudinal spacing between thermocouples located in the vicinity of fire sources is 0.25 m, while the spacing between thermocouples positioned further away from fires on both sides is

0.5 m. Concrete was chosen as the material for the tunnel's walls and ceiling in FDS. The environment has an initial ambient temperature of 20 °C and an atmospheric pressure of 101,325 Pa. To simulate natural ventilation, two ends of the tunnel were configured as open boundaries. Through multiple simulation tests, the duration of the simulation was set to 200 s. A constant heat release rate was chosen for this simulation, and the fire burns for 10 s to reach its maximum heat release rate and then maintains this value for the subsequent simulation time. Figure 1 shows the specific settings of the tunnel numerical model; the relevant specific simulated cases can be seen in Table 1.

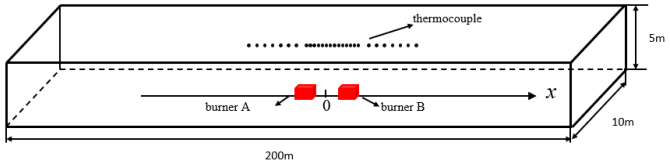

(**a**) The tunnel model and numerical setup

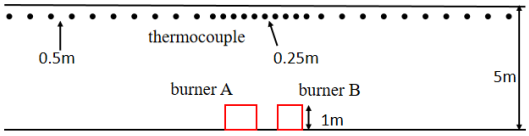

(**b**) Longitudinal section of the model tunnel

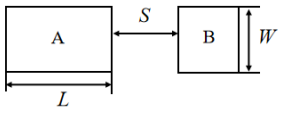

(**c**) Burner setup

Figure 1. Schematic diagram of tunnel model and numerical setup.

Table 1. Summary of simulation tests.

Test No.	Heat Release Rate (MW)	The Dimensions of Burner A ($L \times W$) (m × m)	The Distance between Two Burners (m)
1–30	4 + 4	1 × 1, 1.2 × 1, 1.5 × 1, 1.8 × 1, 2 × 1	0, 0.2, 0.4, 0.6, 0.8, 1, 2
31–60	5 + 5	1 × 1, 1.2 × 1, 1.5 × 1, 1.8 × 1, 2 × 1	0, 0.2, 0.4, 0.6, 0.8, 1, 2
61–90	6 + 6	1 × 1, 1.2 × 1, 1.5 × 1, 1.8 × 1, 2 × 1	0, 0.2, 0.4, 0.6, 0.8, 1, 2

2.2. Grid System

To ensure the precision and accuracy of numerical simulation results, conducting a grid sensitivity analysis is essential when utilizing the Fire Dynamics Simulator (FDS) for fire simulations. Extensive studies have shown that a grid size value between 1/16 to 1/4 of the fire source characteristic diameter is appropriate [36,37]. With this grid size, the calculation results can accurately display the variations of various parameters during the tunnel fire. The fire source feature diameter was represented as:

$$D^* = \left(\frac{\dot{Q}}{\rho_\infty c_p T_\infty \sqrt{g}}\right)^{2/5}, \quad (1)$$

in which D^* represents the feature diameter of the fire; $\dot{Q}$ denotes the heat release rate, kW; ρ_∞ refers to the air density, set at 1.2 kg/m^3; c_p signifies air specific heat, being 1.005 kJ/(kg·K); T_∞ represents ambient temperature, set at 293 K; and g stands for the gravitational acceleration, measured at 9.81 m/s^2. Given that the minimum power of the

fire in present study is 4 MW, the mesh size is accordingly set to range between 0.1 m and 0.45 m. Considering the simulation parameters and duration, four mesh schemes are created for the mesh sensitivity analysis, which can be seen from Table 2.

Table 2. Different grid size schemes.

Grid System	Grid Size in Near-Fire Region	Grid Size in Other Regions	Total Number of Mesh
1	0.2 m × 0.2 m × 0.2 m	0.2 m × 0.2 m × 0.2 m	1,890,000
2	0.25 m × 0.25 m × 0.25 m	0.25 m × 0.25 m × 0.25 m	967,680
3	0.25 m × 0.25 m × 0.25 m	0.5 m × 0.5 m × 0.5 m	524,160
4	0.5 m × 0.5 m × 0.5 m	0.5 m × 0.5 m × 0.5 m	120,960

Figure 2 illustrates the longitudinal TD below the ceiling, considering various grid systems. It reveals that when the grid size below 0.25 m, the temperature distributions closely align. Furthermore, as in Equation (1), an increase in fire source power leads to a larger fire source characteristic diameter, indicating that the grid sensitivity analysis for the 4 MW case can extend to all scenarios covered in this study. After thorough evaluation, Grid System 3 was selected, with a grid size of 0.25 m × 0.25 m × 0.25 m in the vicinity of the fire (20 m on either side of the x_0 coordinate position) and 0.5 m × 0.5 m × 0.5 m in areas further from the fire. This grid system can perform numerical simulations quickly and accurately.

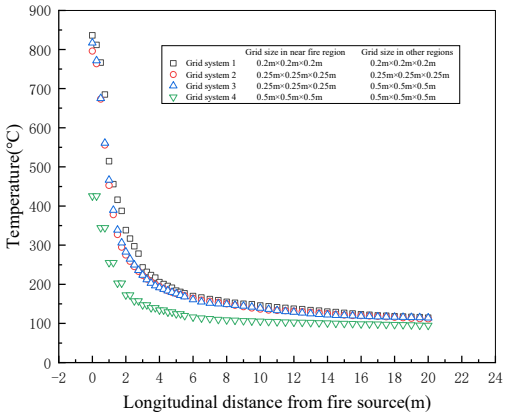

Figure 2. Temperature distribution beneath tunnel ceiling based on four grid systems.

To further ensure the precision of numerical simulation results, one method is to compare the numerical simulation outcomes with previously established dimensionless prediction models. This method is commonly used in full-scale simulation studies.

Heskestad and Hamada constructed a predictive model for the TD below ceiling considering strong plume scenarios based on their research [13]:

$$\begin{gathered}\frac{\Delta T}{\Delta T_{\max}} = 1.92\left(\frac{r}{b}\right)^{-1} - \exp\left[1.61\left(1-\frac{r}{b}\right)\right], 1 \le \frac{r}{b} \le 40, \\ b = 0.42\left[\left(\rho_\infty c_p\right)^{4/5} T_\infty^{3/5} g^{2/5}\right]^{-1/2} \frac{T_{\max}^{1/2}\dot{Q}_c^{2/5}}{\Delta T_{\max}^{3/5}}\end{gathered} \tag{2}$$

In Equation (2), b denotes the plume radius, r represents the horizontal distance from the reference point to the fire center, and $\dot{Q}_c$ represents the convective heat release rate of the fire, as empirically determined as $\dot{Q}_c = 0.8\dot{Q}$ [13]. All fire sources designed in this study were set as strong plume fire sources. In the present study, a comparison of Heskestad's model with the numerical simulation results for a single fire source with a heat release rate of 4 MW is shown in Figure 3, suggesting that the numerical simulation results closely align with the predictions of existing model.

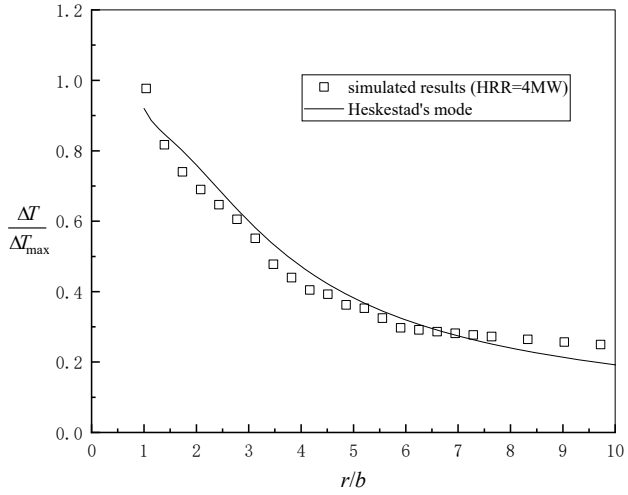

Figure 3. Comparison of numerical results with the predictions based on Heskestad model [13].

3. Results and Discussion

3.1. Longitudinal Temperature Distribution (TD)

Taking the case of a fire source power of 5 MW as an example, Figure 4 shows the longitudinal TD beneath the tunnel ceiling under natural ventilation. The x-coordinate 0 represents the central position between the two burners in the longitudinal direction, and the x-x_0 indicates the reference point to points x_0. The figure shows that the smoke temperature below ceiling decreases as the size of fire source A increases. It is also observed that the side with the increased fire source size shows a more significant decrease in temperature peak. This decrease mainly occurs near the fire sources, with less noticeable temperature changes in areas far from the dual fire sources. Figure 4 illustrates that when the two fire sources distance is small, there is only one peak. However, when both the area of fire A and the fire distance increase, two peaks appear. The two fire sources' interaction decreases with increasing distance between them. In the case of constant power of the fire source, as the area of the fire source increases, the height of the flame decreases. In addition, the air entrainment of the fire plume is enhanced, resulting in a decrease in the temperature of the ceiling. Figure 5 shows the positions where fire plumes hit the tunnel ceiling and the locations of the highest temperatures.

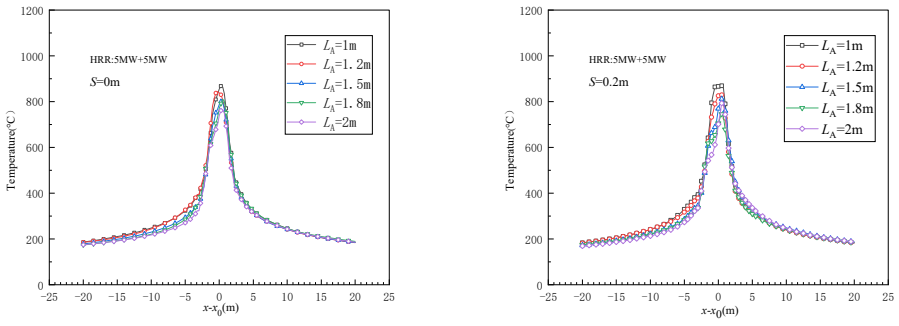

Figure 4. *Cont.*

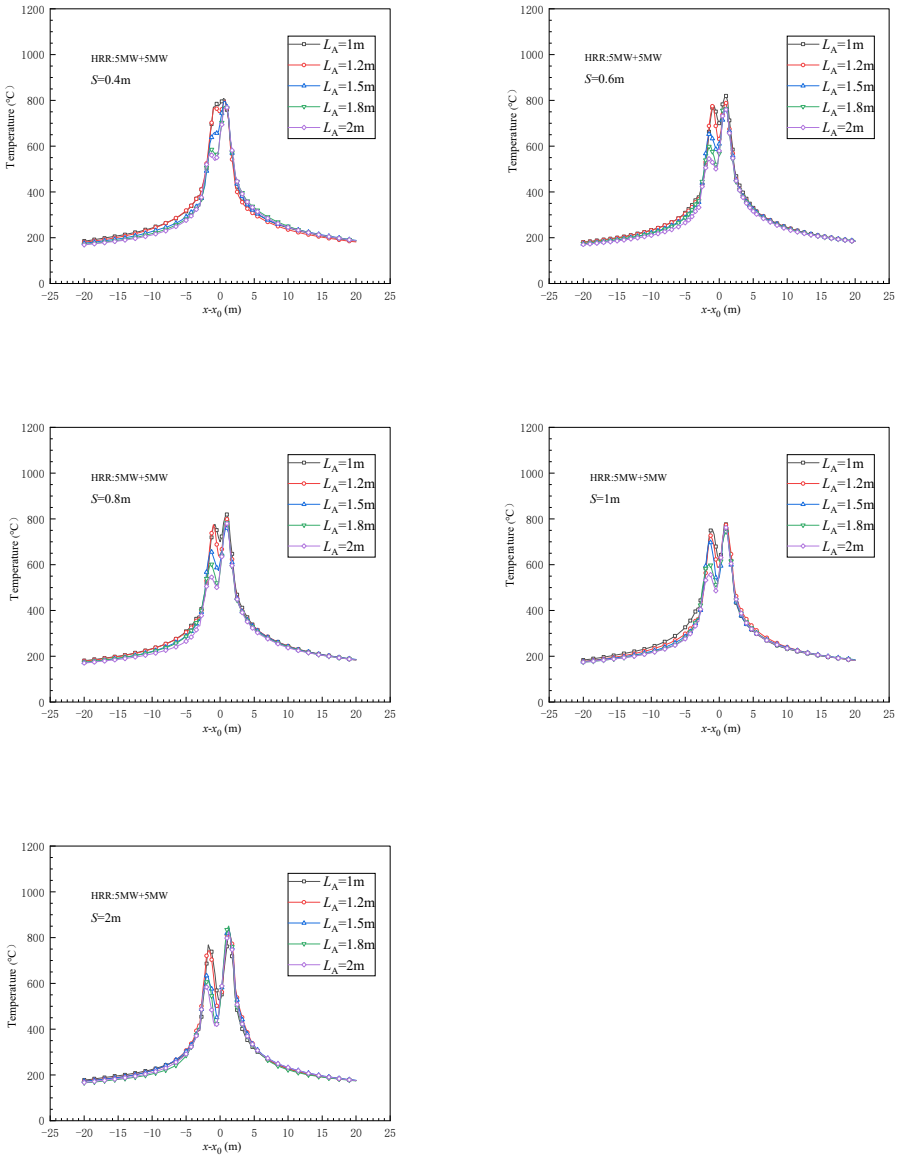

Figure 4. Longitudinal temperature distribution (TD) along the tunnel ceiling.

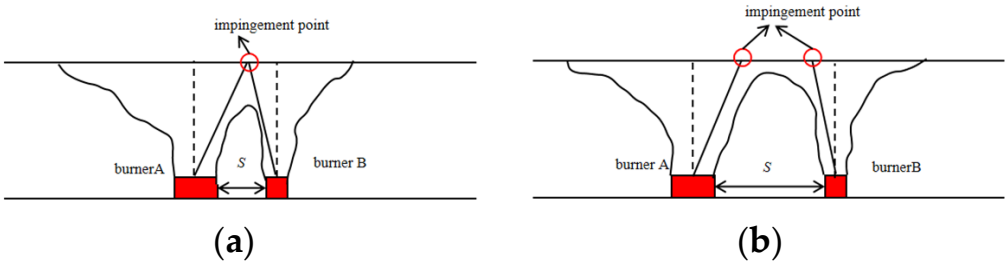

Figure 5. Schematic of the position of impingement point for cases of (**a**) small spacing and (**b**) large spacing.

3.2. Maximum Temperature Modelling

Figure 6 shows the maximum temperature change under different fire source spacings ($\Delta T_{max} = T_{max} - T_{\infty}$), and T_{∞} is expressed as the ambient temperature. From the figure, it can be seen that $\Delta T_{A\text{-}max}$ first reduces and then increases when S is increasing. $\Delta T_{B\text{-}max}$ exhibits a same variation trend with the increase in S as the variation of $\Delta T_{A\text{-}max}$. When the two fire sources distance reaches a threshold, the interaction of two fires decreases, and the MT rise does not change with the increase in fire spacing. When the spacing between

two fire sources is small, the air entrainment of the plume is limited [38]. As the distance increases, the air entrainment of the fire plume is enhanced, which results in a temperature decrease. In cases when the distance between two fire sources is small, the flame plumes tilt inward. As the distance increases, the tilt angle gradually decreases, and eventually the flame burns vertically, which could be the reason for the above mentioned subsequent increase in the maximum temperature rise.

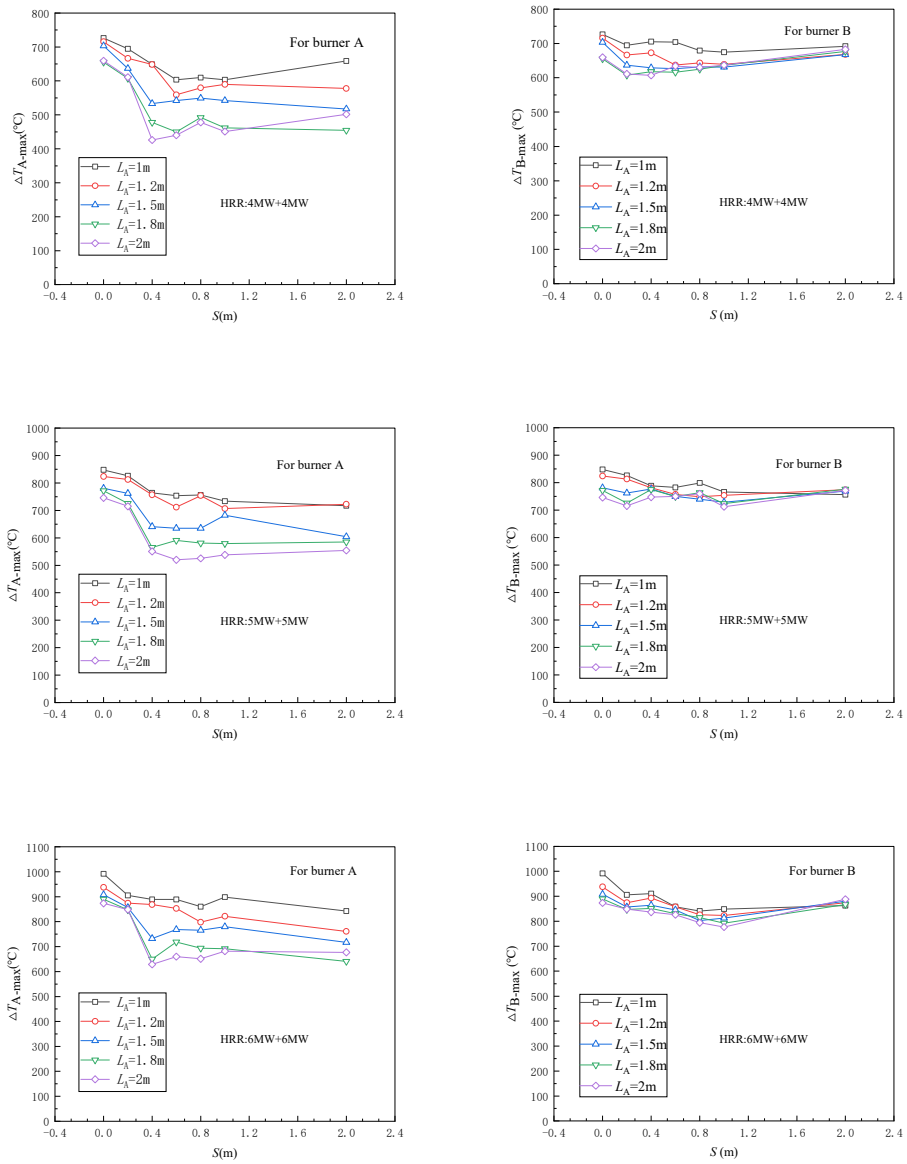

Figure 6. MT against burner spacing.

We will try to establish a model to predict the MT under the ceiling. Previous scholars, in their studies of the MT below the tunnel ceiling [39–42], have developed a model between T_{max}/T_∞ and $\dot{Q}$, the size of the fire (D) and the distance between surface of the fire and ceiling (H_{ef}).

In this study, the tunnel ceiling temperature is associated with a number of factors, including the fire source size, fire source power (HRR), the distance between two fire sources (S) and the distance from fire surface to tunnel ceiling (H_{ef}). Because asymmetric dual fire sources with different areas and shapes are the key research point in this study, and the height of the burner setup does not change, the effect of H_{ef} is not considered when analyzing the maximum temperature.

Considering the interaction of two fire sources, to determine the $\Delta T_{\max}$ of the two sources, the dimensions, spacing and fire power of the two sources should be considered; Wan et al. [22] proposed a dimensionless fire power by analyzing the difference between two different rectangular sources in burner side length, the spacing between two fire sources and the power of fire sources, which is shown as following equation:

$$\dot{Q}_{eq}^{*} = \frac{\dot{Q}_{eq}}{\rho_{\infty} c_p T_{\infty} g^{1/2} D_{eq}^{5/2}} \tag{3}$$

in which $\dot{Q}_{eq}$ refers to the equivalent heat release rate, kW, and D_{eq} means the equivalent size of burner. The equivalent size of the two burners is calculated as:

$$D_{eq} = \gamma D_A + \delta D_B \tag{4}$$

In Equation (4), γ and δ represent the weight values corresponding to the two fire sources, respectively. Here $\gamma + \delta = 1$, and both γ and δ are non-negative. This study focuses on asymmetric dual fire sources with varying sizes and shapes. To facilitate equivalent calculations of their dimensions and account for the varying aspect ratios' impact on the combustion of rectangular fire sources, the concept of perimeter diameter d [43] is introduced to characterize the sizes of the two fire sources. The formula for the perimeter diameter of a rectangular fire source is calculated as follows:

$$d = \frac{2(L + W)}{\pi} \tag{5}$$

According to the ratio of the perimeter diameter of the two fires, the corresponding weight value then is determined. For example, when the length (L_A) of fire source A is 1.5 m, the ratio between the perimeter diameter of the two sources is 14:11, so that the weight value of the characteristic dimensions for the two sources is 0.56 and 0.44. The equivalent dimensions of the two burners can be expressed as:

$$D_{Aeq} = 0.56 d_A + 0.44 d_B \tag{6}$$

$$D_{Beq} = 0.56 d_B + 0.44 d_A \tag{7}$$

Furthermore, the impact of the spacing between asymmetric dual fires is assessed through the introduction of a normalization parameter α [22], as delineated in the following equation:

$$\dot{Q}_{Aeq} = \dot{Q}_A + \alpha_A \dot{Q}_B \tag{8}$$

$$\dot{Q}_{Beq} = \dot{Q}_B + \alpha_B \dot{Q}_A \tag{9}$$

Regarding the parameter α, it is considered that, under condition of the spacing at 0 m, the two fires can be regarded as a unified source, with α being set to 1. As the spacing between the fire sources increases to a sufficient large value, the reciprocal influence diminishes, and α approximates to 0. The value of α is dependent on the dimensions of the fire sources and their spacing. The α decreases with the increase in fire spacing. Thus, α can be formulated as an exponential function, exhibiting a negative correlation with the fire spacing S. Considering the effects of spacing and the size of the fire sources, α is represented by the following equation:

$$\alpha_A = e^{-KS/d_A} \tag{10}$$

$$\alpha_B = e^{-KS/d_B} \tag{11}$$

In the equation, the coefficient in front of S/d (K = 1.5) is based on the assumption adopted by Wan et al. [22]. This study finds that by selecting different K values (ranging

from 0 to 5) for calculating α, the α value ranging from 0 to 1 can be achieved under different conditions when K is set to 1.5.

$$\dot{Q}^*_{Aeq} = \frac{\dot{Q}_A + \alpha_A \dot{Q}_B}{\rho_\infty c_p T_\infty g^{1/2} (\gamma d_A + \delta d_B)^{5/2}} \tag{12}$$

$$\dot{Q}^*_{Beq} = \frac{\dot{Q}_B + \alpha_B \dot{Q}_A}{\rho_\infty c_p T_\infty g^{1/2} (\gamma d_B + \delta d_A)^{5/2}} \tag{13}$$

When the sizes of the two fire sources are the same, Equations (12) and (13) are identical.

Figure 7 illustrates the association between the MT ($\Delta T_{\max}/T_\infty$) and the dimensionless fire source power. It is evident from the figure that all data points are densely distributed. By performing a nonlinear fitting of the data, a predictive model for the MT below ceiling is obtained as shown in Equation (14):

$$\frac{\Delta T_{\max}}{T_\infty} = 3.57 - 3.6 \exp\left(-0.4 \dot{Q}^*_{eq}\right), 1.87 \le \dot{Q}^*_{eq} \le 5.77, \tag{14}$$

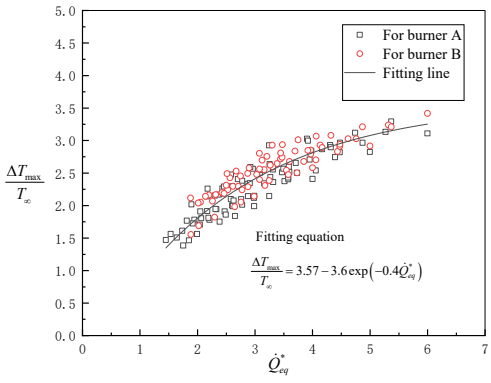

Figure 7. Relationship between $\Delta T_{\max}/T_\infty$ and $\dot{Q}^*_{eq}$.

The tunnel model and fire source settings used in this simulation are similar to the full-scale tunnel model and fire source settings adopted by Ji et al. [18]. By comparing the numerical simulation results with the findings of Ji et al., the outcomes are calculated using Formula (14), as depicted in Figure 8. The proposed model could well predict the MT below ceiling in tunnels featuring asymmetric dual fire sources under conditions of natural ventilation, thereby demonstrating its reliability and applicability to real-world scenarios. Based on the above analysis results, it can be seen that this model can well predict MT in this situation, and the results obtained are consistent with the research results of other scholars, thus demonstrating high practical application value.

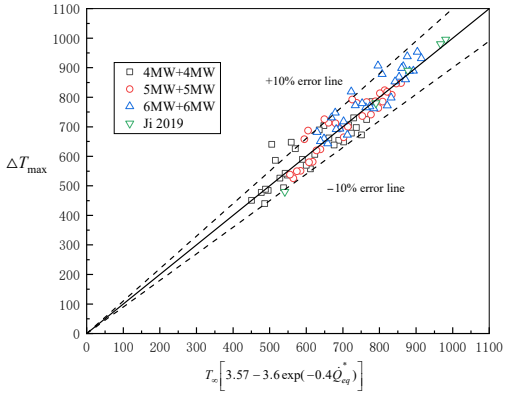

Figure 8. Comparison of predicted results with simulated results and Ji's experimental results [18].

4. Conclusions

This study employs the FDS numerical simulation method to analyze the TD and maximum temperature below tunnel ceiling with asymmetric dual fire sources under natural ventilation. The distance between two fire sources and their sizes were varied. The research finds that the sizes of fire sources and the distance between them could affect the TD and MT below tunnel ceiling. Specific findings include:

1. With the same power of fire source, when the size of one of the fire sources increases, the corresponding maximum temperature beneath ceiling decreases. With the increase in fire spacing, the temperature peak below the ceiling shifts from one to two, and the peak temperature of the larger fire source is lower compared to that of the smaller one.
2. When the fire sources distance increases, the maximum temperature initially decreases and then increases. Beyond a certain distance, the maximum temperature no longer changes with increasing distance.
3. Considering the impact of fire sizes and spacings on the MT, we developed a new predictive model for calculating MT in the case of asymmetric fire sources under a tunnel ceiling. The model performs well in predicting simulation results, showing its novelty and validity for predicting the maximum temperature under case of asymmetric dual fire sources.

In present research, we studied the TD and MT beneath the ceiling induced by a ceiling jet of asymmetric dual fire sources in a naturally ventilated tunnel, by varying the size and spacing of the fire. Nevertheless, this article still has certain shortcomings. For the burner setup, only rectangular burners were used, and they were positioned exclusively along the tunnel's centerline. However, in reality, tunnel fire scenarios are far more complex. Future studies will explore asymmetric dual fire sources, focusing on different shapes and locations. In this paper, we only obtained the prediction model for MT, and the temperature decay along the tunnel ceiling was not analyzed deeply, which will continue to be researched in future research. Additionally, the tunnel model cross-section adopted in this simulation is rectangular, and it is necessary to conduct investigations with different cross-sections in future research.

Author Contributions: Conceptualization, S.Z. and N.M.; methodology, S.Z. and N.M.; software, S.Z.; validation, S.Z.; formal analysis, S.Z.; investigation, S.Z.; resources, S.Z.; data curation, S.Z.; writing—original draft preparation, S.Z.; writing—review and editing, S.Z. and N.M.; supervision, N.M.; project administration, N.M.; funding acquisition, N.M. All authors have read and agreed to the published version of the manuscript.

Funding: This research was funded by the National Natural Science Foundation of China, grant number 51974175.

Institutional Review Board Statement: Not applicable.

Informed Consent Statement: Not applicable.

Data Availability Statement: Data are contained within the article.

Conflicts of Interest: The authors declare no conflicts of interest.

References

1. Fridolf, K.; Nilsson, D.; Frantzich, G. Fire evacuation in underground transportation systems: A review of accidents and empirical research. *Fire Technol.* **2013**, *49*, 451–475. [CrossRef]
2. Gehandler, J. Road tunnel fire safety and risk: A review. *Fire Sci. Rev.* **2015**, *4*, 2. [CrossRef]
3. Carvel, R. A review of tunnel fire research from Edinburgh. *Fire Saf. J.* **2019**, *105*, 300–306. [CrossRef]
4. Arends, B.J.; Jonkman, S.N.; Vrijling, J.K.; van Gelder, P.H.A.J.M. Evaluation of tunnel safety: Towards an economic safety optimum. *Reliab. Eng. Syst. Saf.* **2005**, *90*, 217–228. [CrossRef]
5. Amundsen, F.H.; Ranes, G. Studies on traffic accidents in Norwegian road tunnels. *Tunn. Undergr. Space Technol.* **2000**, *15*, 3–11. [CrossRef]
6. Haule, H.J.; Sando, T.; Lentz, R.; Chuan, C.H.; Alluri, P. Evaluating the impact and clearance duration of freeway incidents. *Int. J. Transp. Sci. Technol.* **2009**, *8*, 13–24. [CrossRef]
7. Miclea, P.C.; Chow, W.K.; Shen-Wen, C.; Junmei, L.; Kashef, A.; Kang, K. International tunnel fire-safety design practices. *ASHRAE J.* **2007**, *49*, 50–60.
8. Oka, Y.; Atkinson, G.T. Control of smoke flow in tunnel fires. *Fire Saf. J.* **1995**, *25*, 305–322. [CrossRef]
9. Kodur, V.; Naser, M.Z. Fire hazard in transportation infrastructure: Review, assessment, and mitigation strategies. *Front. Struct. Civ. Eng.* **2021**, *15*, 46–60. [CrossRef]
10. Bernardi, P.; Michelini, E.; Sirico, A.; Rainieri, S.; Corradi, C. Simulation methodology for the assessment of the structural safety of concrete tunnel linings based on CFD fire—FE thermo-mechanical analysis: A case study. *Eng. Struct.* **2020**, *225*, 111193. [CrossRef]
11. Maraveas, C.; Vrakas, A.A. Design of Concrete Tunnel Linings for Fire Safety. *Struct. Eng. Int.* **2014**, *24*, 319–329. [CrossRef]
12. Alpert, T.R. Calculation of response time of ceiling-mounted fire detectors. *Fire Technol.* **1972**, *8*, 181–195. [CrossRef]
13. Heskestad, G.; Hamada, T. Ceiling jets of strong fire plumes. *Fire Saf. J.* **1993**, *21*, 69–82. [CrossRef]
14. Ingason, H.; Li, Y.Z. Model scale tunnel fire tests with longitudinal ventilation. *Fire Saf. J.* **2010**, *45*, 371–384. [CrossRef]
15. Kurioka, H.; Oka, Y.; Satoh, H.; Sugawa, O. Fire properties in near field of square fire source with longitudinal ventilation in tunnels. *Fire Saf. J.* **2003**, *38*, 319–340. [CrossRef]
16. Zhang, X.; Lin, Y.; Shi, C.; Zhang, J. Numerical simulation on the maximum temperature and smoke back-layering length in a tilted tunnel under natural ventilation. *Tunn. Undergr. Space Technol.* **2021**, *107*, 103661. [CrossRef]
17. Caliendo, C.; Genovese, G.; Russo, I. A 3D CFD modeling for assessing the effects of both longitudinal slope and traffic volume on user safety within a naturally ventilated road tunnel in the event of a fire accident. *IATSS Res.* **2022**, *46*, 547–558. [CrossRef]
18. Ji, J.; Tan, T.T.; Gao, Z.H.; Wan, H.X.; Zhu, Z.P.; Ding, L. Numerical investigation on the influence of length-width ratio of fire source on the smoke movement and temperature distribution in tunnel fires. *Fire Technol.* **2019**, *55*, 963–979. [CrossRef]
19. Gao, Z.; Li, L.; Sun, C.; Zhong, W.; Yan, C. Effect of longitudinal slope on the smoke propagation and ceiling temperature characterization in sloping tunnel fires under natural ventilation. *Tunn. Undergr. Space Technol.* **2022**, *123*, 104396. [CrossRef]
20. Zhou, Y.; Chen, F.; Geng, Z.Y.; Bu, R.W.; Gong, W.X.; Fan, C.G.; Yi, L. Experimental study on the characteristics of temperature distribution of two pool fires with different transverse locations in a naturally ventilated tunnel. *Tunn. Undergr. Space Technol.* **2021**, *116*, 104095. [CrossRef]
21. Zhang, Y.C.; Xing, S.S.; Chen, R.J.; Chen, L.F.; Li, T.; Mao, P.F. Experimental study on maximum temperature beneath tunnel ceiling under the condition of double fire sources. *Tunn. Undergr. Space Technol.* **2020**, *106*, 103624. [CrossRef]
22. Wan, H.X.; Xiao, Y.Y.; Wei, S.Q.; Zhang, Y.C. Performance of ceiling jet induced by dual unequal strong plumes in a naturally ventilated tunnel. *Appl. Therm. Eng.* **2022**, *211*, 118447. [CrossRef]
23. Meng, N.; Shu, Y.M.; Zhang, S.H. Study on smoke temperature induced by two fires in a naturally ventilated tunnel. *Tunn. Undergr. Space Technol.* **2023**, *131*, 104774. [CrossRef]
24. Wang, Q.; Wang, S.M.; Liu, H.; Sheng, J.Y.; Shang, F.J.; Shi, C.L.; Tang, F. Characterization of ceiling smoke temperature profile and maximum temperature rise induced by double fires in a natural ventilation tunnel. *Tunn. Undergr. Space Technol.* **2020**, *96*, 103233. [CrossRef]
25. Jia, Y.; Fan, X.L.; Zhao, X.J.; Deng, Y.L.; Zhu, X.L.; Zhao, W.F. Study on the longitudinal ceiling temperature distribution induced by double pool fires in a tunnel. *Int. J. Therm. Sci.* **2021**, *168*, 107059. [CrossRef]
26. Zhao, J.L.; Cui, X.Y.; Yao, Y.Z.; Yang, R.; Chen, C.K. The burning process and temperature profile of double fires in a tunnel: An experimental study. *Tunn. Undergr. Space Technol. Inc. Trench. Technol. Res.* **2022**, *125*, 104500. [CrossRef]
27. Heidarinejad, G.; Mapar, M.; Pasdarshahri, H. A comprehensive study of two fire sources in a road tunnel: Considering different arrangement of obstacles. *Tunn. Undergr. Space Technol.* **2016**, *59*, 91–99. [CrossRef]
28. Clement, J.M.; Fleischmann, C.M. Experimental verification of the Fire dynamics simulator (FDS) hydrodynamic model. *Fire Saf. Sci.* **2003**, *7*, 839–850. [CrossRef]
29. Beji, T.; Bonte, F.; Merci, B. Numerical simulations of a mechanically-ventilated multi-compartment fire. *Fire Saf. Sci.* **2014**, *11*, 499–509. [CrossRef]

30. Gannouni, S.; Zinoubi, J.; Maad, R.B. Numerical study on the thermal buoyant flow stratification in tunnel fires with longitudinal imposed airflow: Effect of an upstream blockage. *Int. J. Therm. Sci.* **2019**, *136*, 230–242. [CrossRef]
31. Oliveira, R.L.F.; Doubek, G.; Vianna, S.S.V. On the behaviour of the temperature field around pool fires in controlled experiment and numerical modelling. *Process Saf. Environ. Prot.* **2019**, *123*, 358–369. [CrossRef]
32. Brohez, S.; Caravita, I. Fire induced pressure in airthigh houses: Experiments and FDS validation. *Fire Saf. J.* **2020**, *114*, 103008. [CrossRef]
33. Xu, H.S.; Lin, K.; Mao, S.H.; Wang, J.; Ding, Y.M.; Lu, K.H. Numerical investigation of air curtain jet effect upon the compartment-facade fire safety protection based on temperature evolution and thermal impact. *Therm. Sci. Eng. Prog.* **2023**, *43*, 101988. [CrossRef]
34. Ma, T.G.; Quintiere, J.G. Numerical simulation of axisymmetric fire plumes: Accuracy and limitations. *Fire Saf. J.* **2003**, *38*, 467–492. [CrossRef]
35. Oka, Y.; Kurioka, H. Effect of Shape and Size of a Fire Source on Fire Properties in Vicinity of a Fire Source in a Tunnel. *Fire Sci. Technol.* **2006**, *25*, 15–29. [CrossRef]
36. McGrattan, K.; McDermott, R.; Weinschenk, C.; Forney, G. *Fire Dynamics Simulator Users Guide*, 6th ed.; Special Publication (NIST SP); National Institute of Standards and Technology: Gaithersburg, MD, USA, 2013.
37. McGrattan, K.; McDermott, R.; Weinschenk, C.; Overholt, K.; Hostikka, S.; Floyd, J. *Fire Dynamics Simulator Technical Reference Guide Volume 1: Mathematical Model (NIST SP)*; National Institute of Standards and Technology: Gaithersburg, MD, USA, 2013.
38. Zukoski, E.E.; Kubota, T.; Cetegen, B. Entrainment in Fire Plumes. *Fire Saf. J.* **1981**, *3*, 107–121. [CrossRef]
39. Alpert, T.R. Turbulent ceiling-jet induced by large-scale fires. *Combust. Combust. Sci. Technol.* **1975**, *11*, 197–213. [CrossRef]
40. Haghighat, A.; Luxbacher, K. Determination of critical parameters in the analysis of road tunnel fires. *Int. J. Min. Sci. Technol.* **2019**, *29*, 187–198. [CrossRef]
41. Cooper, L.Y.; Woodhouse, A. The buoyant plume-driven adiabatic ceiling temperature revisited. *J. Heat Transf.* **1986**, *108*, 822–826. [CrossRef]
42. Motevalli, V. Numerical prediction of ceiling jet temperature profiles during ceiling heating using empirical velocity profiles and turbulent continuity and energy equations. *Fire Saf. J.* **1994**, *22*, 125–144. [CrossRef]
43. Tang, F.; Hu, P.; Wen, J. Experimental investigation on lateral ceiling temperature distribution induced by wall- attached fire with various burner aspect ratios in underground space. *Fire Saf. J.* **2021**, *120*, 103055. [CrossRef]